Research in Astron. Astrophys. **2011** Vol. **11** No. **8**, 924–946
http://www.raa-journal.org *http://www.iop.org/journals/raa*

Research in Astronomy and Astrophysics

Automatic determination of stellar atmospheric parameters and construction of stellar spectral templates of the Guoshoujing Telescope (LAMOST) *

Yue Wu[1,2,3,4], A-Li Luo[1,3,5], Hai-Ning Li[1,3], Jian-Rong Shi[1,3], Philippe Prugniel[2], Yan-Chun Liang[1,3], Yong-Heng Zhao[1,3,5], Jian-Nan Zhang[1,3], Zhong-Rui Bai[1,3], Peng Wei[5,1,3], Wei-Xiang Dong[5,1,3], Hao-Tong Zhang[1,3] and Jian-Jun Chen[1,3]

[1] National Astronomical Observatories, Chinese Academy of Sciences, Beijing 100012, China; *wuyue@lamost.org, lal@lamost.org*
[2] Université de Lyon, Université Lyon 1, Villeurbanne, F-69622, France; CRAL, Observatoire de Lyon, CNRS UMR 5574, 69561 Saint-Genis Laval, France;
[3] Key Laboratory of Optical Astronomy, NAOC, Chinese Academy of Sciences;
[4] Graduate University of Chinese Academy of Sciences, Beijing 100049, China
[5] Shandong University at Weihai, Weihai 264209, China

Received 2010 July 15; accepted 2010 September 21

Abstract A number of spectroscopic surveys have been carried out or are planned to study the origin of the Milky Way. Their exploitation requires reliable automated methods and softwares to measure the fundamental parameters of the stars. Adopting the ULySS package, we have tested the effect of different resolutions and signal-to-noise ratios (SNR) on the measurement of the stellar atmospheric parameters (effective temperature $T_{\rm eff}$, surface gravity $\log g$, and metallicity [Fe/H]). We show that ULySS is reliable for determining these parameters with medium-resolution spectra ($R \sim$2000). Then, we applied the method to measure the parameters of 771 stars selected in the commissioning database of the Guoshoujing Telescope (LAMOST). The results were compared with the SDSS/SEGUE Stellar Parameter Pipeline (SSPP), and we derived precisions of 167 K, 0.34 dex, and 0.16 dex for $T_{\rm eff}$, $\log g$ and [Fe/H] respectively. Furthermore, 120 of these stars are selected to construct the primary stellar spectral template library (Version 1.0) of LAMOST, and will be deployed as basic ingredients for the LAMOST automated parametrization pipeline.

Key words: astronomical data bases: atlases — stars: fundamental parameters — techniques: spectroscopic — surveys

1 INTRODUCTION

The origin and evolution of the Milky Way are key subjects in modern astrophysics. To explore these subjects, it is essential to understand the intrinsic properties, such as stellar masses, ages, chemical abundances, and kinematics for statistically significant samples of stars in the Galaxy. They will

* Supported by the National Natural Science Foundation of China.

be used to match the structure and evolution of the Milky Way to the current generation of galaxy formation models (Wyse 2006; Jurić et al. 2008; Ivezić et al. 2008; Bond et al. 2010; Jofre & Weiss 2011).

Thanks to the development of astronomical technology and instruments, e.g., multi-fiber and multi-aperture spectrographs, adaptive optics, etc., large survey projects have become possible. These include the successful projects such as the Sloan Digital Sky Survey (SDSS, York et al. 2000), the follow-up Sloan Extension for Galactic Understanding and Exploration (SEGUE, Yanny et al. 2009) and SEGUE-2 (Rockosi et al. 2009), as well as ongoing surveys such as the Radial Velocity Experiment (RAVE, Steinmetz et al. 2006; Zwitter et al. 2008; Siebert et al. 2011), the Guoshoujing Telescope [1] — the Large sky Area Multi-Object fiber Spectroscopic Telescope (LAMOST) survey, SDSS-III[2], and a number of surveys which are being planned, e.g., Galactic (GAIA, Perryman et al. 2001), APOGEE (Schiavon & Majewski 2010) and HERMES (Wylie-de Boer & Freeman 2010). Unprecedentedly large spectroscopic databases of Galactic stars are becoming available.

This data avalanche calls for new analysis tools for automated and efficient parameterizations of stellar spectra. The basic atmospheric parameters, $T_{\rm eff}$, $\log g$, and [Fe/H], are some of the characteristics that the analysis pipelines of the spectroscopic surveys shall determine. Many research teams have made great efforts in this field, aiming to efficiently and reliably extract the maximal amount of astrophysical information, especially to determine the atmospheric parameters over wide ranges of $T_{\rm eff}$, $\log g$, and [Fe/H]. Numerous methods have been developed in order to extract those atmospheric parameters from medium-resolution stellar spectra in a fast, automatic, objective fashion. Generally, these approaches can be sorted into two main categories, the minimum distance method (MDM), and the non-linear regression method, commonly called Artificial Neural Network or ANN. Except for the above two main categories, there are other methods, like correlations between broad-band colors or the strength of prominent metallic lines and the atmospheric parameters (Beers et al. 1999; Wilhelm et al. 1999; Cenarro et al. 2001a,b; Alonso et al. 1996b,a, 1999a,b; Ivezić et al. 2008; An et al. 2009; Árnadóttir et al. 2010).

MDM has been widely used in the past, not only for the automatic parametrization of $T_{\rm eff}$, $\log g$, [Fe/H], radial velocity, etc., but also for spectral classification. The solution is based on the best matching template spectrum according to the shortest distance in an N-dimensional data space, where N is the number of selected spectral features. To use this kind of method, first, we need to construct a stellar spectral template library with which accurate parameters have been previously determined via traditional methods. The χ^2 minimization, the cross-correlation, the weighted average algorithm, and the k-nearest neighbor (KNN) method, etc., are various specific cases of the MDM. There are many representative works assigned in this category. For example, Katz et al. (1998) developed the TGMET software to derive parameters by a direct comparison with a reference library of stellar spectra. This work was later updated by Soubiran et al. (2000, 2003) to an internal accuracy of 86 K, 0.28 dex and 0.16 dex respectively for $T_{\rm eff}$, $\log g$ and [Fe/H] for F, G and K stars with SNR = 100, and accuracy of 102 K, 0.29 dex and 0.17 dex at SNR = 10. In Zwitter et al. (2008), the parameters are derived by a penalized χ^2 method using an extensive grid of synthetic spectra calculated from the latest version of Kurucz stellar atmospheric models. There are many other typical works in this category, including Zwitter et al. (2005), MATISSE (Recio-Blanco et al. 2006), Allende Prieto et al. (2006), Shkedy et al. (2007), Jofré et al. (2010), as well as the SSPP (Lee et al. 2008a), in which they employed various techniques in integrated approaches containing both MDM and ANN methods.

Meanwhile, a number of early studies have demonstrated that ANN methods can be robust and precise for parametrization, by providing a functional mapping between the spectra as their inputs and the parameters as their outputs. The optimal mapping is found by training the network (i.e.

[1] *http://www.lamost.org/website/en/*

[2] *http://www.sdss3.org/*

setting its weights) on a set of either pre-classified observed stellar spectra or synthetic stellar spectra (both used as templates). Re Fiorentin et al. (2007) succeeded in deriving atmospheric parameters from medium-resolution stellar spectra using non-linear regression models which can be trained alternatively on either real observations or synthetic spectra. By comparing with the SDSS/SEGUE data, they reached RMS deviations on the order of 150 K in $T_{\rm eff}$, 0.35 dex in $\log g$, and 0.22 dex in [Fe/H]. Similar efforts can be found in SSPP (Lee et al. 2008a), Bailer-Jones et al. (1997); Bailer-Jones (2000); Willemsen et al. (2005); Zhao et al. (2006) and Manteiga et al. (2010).

For both techniques, a comprehensive set of reference spectra with known atmospheric parameters is crucial. Such *stellar spectral libraries* with medium to high resolution and good coverage of the Hertzsprung-Russell diagram are also an essential tool in several areas of astronomy, including:

(1) Automated classification and parametrization of large volumes of stellar spectral data, especially those collected by ongoing large spectroscopic surveys;
(2) Spectral synthesis of stellar populations of galaxies, e.g. Le Borgne et al. (2004); Percival & Salaris (2009); Prugniel et al. (2007a); Koleva et al. (2007); Vazdekis et al. (2010), and Chen et al. (2010);
(3) Derivation of radial velocities via cross-correlation against the best matched templates, e.g. Tonry & Davis (1979); Valentini & Munari (2010);
(4) Calibration of spectroscopic line/band classification criteria;
(5) Calibration of photometric indices.

The larger quantity and better quality of newly obtained spectra have promoted improvements of these libraries, and nowadays the empirical and synthetic stellar spectral libraries are developed in parallel. For the former ones, the spectra are the real observations ideally collected with a single instrumentation setup. Some popular empirical libraries are ELODIE (Prugniel & Soubiran 2001, 2004; Prugniel et al. 2007b); UVES-POP (Bagnulo et al. 2003); STELIB (Le Borgne et al. 2003); CFLIB (The INDO-US library of Coudé-feed Stellar Spectra, Valdes et al. 2004); MILES (Sánchez-Blázquez et al. 2006; Cenarro et al. 2007); and NGSL (Heap & Lindler 2007). For the latter ones, the spectra are calculated with a stellar model atmosphere, e.g. ATLAS9 (Kurucz 1993), Kurucz 2003 (Castelli & Kurucz 2003), MARCS (Gustafsson et al. 2008), Short & Hauschildt (2010), and lists of atomic and molecular lines, e.g. Cayrel et al. (1991); Barbuy et al. (2003). Some important synthetic libraries are BaSeL (Lastennet et al. 2002); a grid of synthetic spectra and indices for Fe I 5270, Fe I 5335, Mg Ib and $\rm Mg_2$ as a function of stellar parameters and [α/Fe] (Barbuy et al. 2003); a library of high-resolution Kurucz spectra in the range λ 3000–10 000 Å (Murphy & Meiksin 2004); an extensive library of 2500–10 500 Å synthetic spectra (Munari et al. 2005); a high-resolution stellar library for evolutionary population synthesis (Martins et al. 2005); a library of high resolution synthetic stellar spectra from 300 nm to 1.8 μm with solar and α-enhanced composition (Coelho et al. 2005); UVBLUE (Rodríguez-Merino et al. 2005); and synthetic stellar and SSP libraries as templates for Gaia simulations (Sordo et al. 2010). All these libraries widely differ in the number of stars, the calibration quality, wavelength intervals, spectral resolution, range of atmospheric parameters, etc.

The choice between the use of empirical or synthetic libraries is a subject of debate in the literature. The advantage of the observed libraries is that they are *real*, hence avoiding any simplifying assumptions in the synthetic spectra calculation (Munari et al. 2001), but the limitation is the inability to extrapolate to abundance patterns differing from those of the input stars. The synthetic libraries can overcome this limitation by providing a more uniform coverage in the parameter space, but the problem remains that they depend on model atmospheres, with potential systematic uncertainties. For example, Kurucz models (Kurucz 1993; Castelli & Kurucz 2003) assume local thermodynamic equilibrium, which is known to break down in a number of regimes (e.g. for very hot stars). Besides, $T_{\rm eff}$, $\log g$, and [Fe/H] do not uniquely describe a true spectrum, hence advanced models that are sensitive to different abundance ratios and concerning, e.g., chromospheres/dust are necessary.

The LAMOST (Su et al. 1998; Xing et al. 1998; Zhao 2000; Zhu et al. 2006) is a unique astronomical instrument for large area spectroscopic survey. It can simultaneously obtain spectra of 4000 celestial objects due to its special multi-fiber design. Since 2009, LAMOST has initiated its commissioning stage, which mainly consists of tests on its reliability and stability, and adjustments for optimized performance and operation. One of the major scientific aims of the LAMOST project is to study the formation and evolution of our Galaxy. The observed stars are expected to include almost all evolutionary stages and a wide range of masses in the Hertzsprung-Russell diagram.

To achieve the above scientific goal, a prerequisite is the quality of the LAMOST 1D stellar parameter pipeline (Luo et al. 2008, using a non-linear regression method), which is responsible for automatic spectral classification and parametrization. Obviously, a major element is the database of stellar spectral templates. We plan to take a representative set of observed stellar spectra across the entire parameter space, determine accurate atmospheric parameters, and adopt these spectra to train the parameterizers. We will build this database with LAMOST spectra in order to suppress the effects due to observational signatures. We will assemble a first version of this template library using the data acquired during the commissioning period. In this paper, we employ ULySS to automatically determine the stellar atmospheric parameters, test the accuracy of the measurements, and present a first version of the LAMOST template library. The observation and data reduction are described in Section 2. Methods for the determination of the stellar atmospheric parameters and their validation are presented in Section 3. The adopted parameters of the selected LAMOST commissioning spectra are described in Section 4. Our proposed stellar spectral templates are provided in Section 5, and our summary and further prospects are discussed in Section 6.

2 OBSERVATION AND DATA REDUCTION

At the time our sample was assembled, the LAMOST was still in its engineering commissioning phase and subject to instrumental instability. In order to maintain homogeneity as much as possible, we adopted the spectra observed in one LAMOST commissioning field on 2010 February 13. Most of the observations are field stars around M67. The input targets were taken from the UCAC3 (Zacharias et al. 2010) catalog with R band magnitudes brighter than 16.5. The observations were done with double exposures of 30 minutes and 20 minutes respectively, and a seeing of $\sim 3.3''$ (FWHM of the CCD image of the guide star)[3].

The resolving mode $R = 2000$ was adopted. It was achieved by setting the slit width to half of the diameter of the fibers, which inevitably leads to losing 39% of the incoming light (the percentage of the cross section area which was blocked). This sacrifice is the price to enhance the resolution that would be around $R =$1000 otherwise. The spectral coverage was between 370–590 nm and 570–900 nm for the blue and red arms of the spectrographs, respectively. Four thousand fibers were allocated to 16 spectrographs, from No.1 through No.16. However, due to the design of the LAMOST, fibers closer to the center of the focal plane suffered less vignetting and hence showed better image quality. Therefore, our selection was biased against targets located at the outer region of the focal plane. In addition, the present relatively low optical efficiency, inaccuracy in fiber positioning, and uncertainties in the flat-fielding and sky-subtraction lead to a large number of low-quality spectra. We further excluded spectra with SNR less than 10. Out of the 4000 observed objects, the above selection yielded a final sample of 771 stars; these data will be analyzed and adopted as basic ingredients to construct the preliminary stellar spectral template library for LAMOST. Note that data of some selected objects showed only one exposure with good quality while others were acceptable in both exposures. For the latter case, the two observations were combined to enhance the SNR. The

[3] At that time, the dome seeing conditions of the LAMOST were not ideal. At present, work is ongoing to improve this situation by adjusting the ventilation and cryogenic systems of the interior of the dome and the telescope tube. In the near future, we will continue to correct the comparatively large temperature difference of the Ma mirror, Mb mirror and the focal plane of the LAMOST, e.g. by employing refrigeration at these locations.

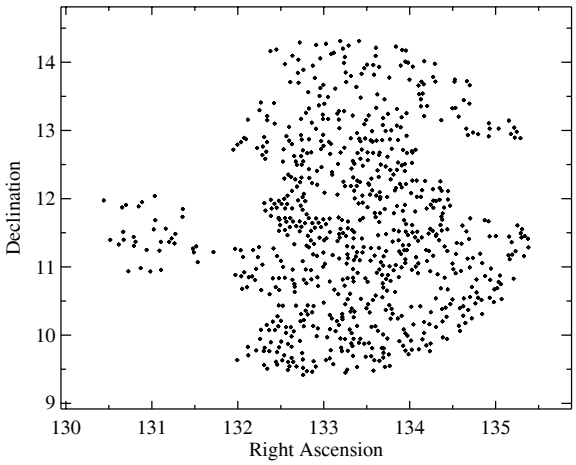

Fig. 1 Projection of the selected 771 LAMOST stellar observations in equatorial coordinates.

coordinates and R band magnitudes of the selected objects are listed in Table 1 (Only five objects were shown. The full table is only available in the electronic version *http://www.raa-journal.org*). R band magnitudes of the selected sample are between 7.29 and 16.37, and the spatial distribution is shown in Figure 1.

Table 1 ULySS Determined Atmospheric Parameters for the Selected LAMOST Stars Observed During its Commissioning Period.

Sp	Fib	RA	Dec	R Mag	$T_{\rm eff}$ (K)	error	$\log g$ ($\rm cm\ s^{-2}$)	error	[Fe/H] (dex)	error	Flag
(1)	(2)	(3)	(4)	(5)	(6)	(7)	(8)	(9)	(10)	(11)	(12)
1	3	132.8668060	9.4641514	13.74	4823	± 37	4.63	± 0.13	–0.38	± 0.13	0
1	6	133.0262909	9.6342649	14.22	5724	± 48	4.31	± 0.19	–0.25	± 0.13	0
1	10	133.0710449	9.6591053	13.33	5295	± 41	4.50	± 0.16	–0.32	± 0.13	0
1	17	133.1125793	9.5741863	14.79	5128	± 55	4.66	± 0.19	–0.24	± 0.18	0
1	20	132.8823700	9.6176205	13.98	5455	± 45	4.60	± 0.16	0.11	± 0.13	0
...	...	...	...	...	...	...	...	...	...	...	...

Notes: This printed version features only five stellar atmospheric parameters determined by ULySS. The full table, which includes all the 771 stars, is only available in the electronic version. 'Sp' is the number of the spectrography, and 'Fib' is the fiber ID number. The third and fourth columns are the RA and DEC. The fifth column is the R band magnitude. The last column is a flag indicating if it is a spectrum selected as a member of the stellar spectral template library, '0', not a member of the library; '1', a member of the library.

The raw data were reduced with the LAMOST standard 2D pipeline (Luo et al. 2004), including bias subtraction, cosmic-ray removal, 1D spectral trace and extraction, flat-fielding, wavelength calibration, and sky subtraction. Since the flux calibration was not yet reliable, this step was not implemented in our sample spectra.

3 APPLICATION AND VALIDATION OF ULYSS TO ATMOSPHERIC PARAMETER DETERMINATION WITH STELLAR SPECTRA AT R =2000

In this work, we employed ULySS[4] (Université de Lyon Spectroscopic analysis Software, Koleva et al. 2009a,b); to analyze the selected spectra. This package is written in the Interactive Data

[4] available at: *http://ulyss.univ-lyon1.fr*

Language (IDL) and enables full spectral fitting for various astrophysical applications, including the determination of (i) stellar atmospheric parameters, e.g., the TGM case, where T, G and M respectively represent the effective temperature, the surface gravity and the metallicity (Wu et al. 2011; Prugniel et al. 2011a; Koleva et al. 2009a), and (ii) the star formation and metal enrichment history of galaxies, e.g., SSP (simple stellar population) case (Michielsen et al. 2007; Koleva et al. 2009b; Bouchard et al. 2010; Makarova et al. 2010; Smirnova & Moiseev 2010; Sharina et al. 2010). It minimizes χ^2 between an observed spectrum and a model spectrum, and the fit is performed in the pixel space (evenly sampled in logarithm of wavelength). The method determines all the free parameters in a single fit in order to properly handle the degeneracy between the temperature and the metallicity. This method has already been successfully tested in Wu et al. 2011. In this section, we will briefly introduce the usage of ULySS to determine the stellar atmospheric parameters using medium-resolution spectra (e.g. obtained by SDSS and LAMOST). We evaluate the effect of the resolution and SNRs.

3.1 ULySS Method

In ULySS, an observed spectrum is fitted against a model expressed as a linear combination of non-linear components, optionally convolved with a line-of-sight velocity distribution (LOSVD) and multiplied with a polynomial function. A component is a non-linear function of some physical parameters, e.g., $T_{\rm eff}$, $\log g$ and [Fe/H] for the TGM case. The multiplicative polynomial is meant to absorb errors in the flux calibration, Galactic extinction or any other source affecting the shape of the spectrum. It replaces the prior *rectification* or normalization to the pseudo-continuum that other methods require, as in Valentini & Munari (2010). This model is compared to the data through a non-linear least-square minimization. The minimization issue can be written as

$$\mathrm{Obs}(\lambda) = P_n(\lambda) \times [\mathrm{TGM}(T_{\rm eff}, \log g, [\mathrm{Fe/H}], \lambda) \otimes G(v_{\rm sys}, \sigma)],$$

where $\mathrm{Obs}(\lambda)$ is the observed stellar spectrum (λ is the logarithm of the wavelength), $P_n(\lambda)$ a development in Legendre polynomials of order n, and $G(v_{\rm sys}, \sigma)$ is a Gaussian broadening function characterized by the systemic velocity $v_{\rm sys}$, and the dispersion σ. The free parameters of the minimization process are the three parameters of the TGM function ($T_{\rm eff}$, $\log g$ and [Fe/H]), the two parameters of the Gaussian ($v_{\rm sys}$ and σ), and the coefficients of P_n. $v_{\rm sys}$ absorbs the imprecision of the cataloged radial velocity of the stars which were used to reduce them in the rest frame; σ encompasses both the instrumental broadening and the effects of stellar rotation.

The TGM function is an *interpolator* of the ELODIE library (Prugniel & Soubiran 2001, 2004; Prugniel et al. 2007a) version 3.2 (Wu et al. 2011; Prugniel et al. 2011b in preparation), which has a wavelength coverage of 3900Å–6800Å, and a resolution ability in the version of $R = 10\,000$. The interpolator consists of polynomial expansions of each wavelength element in powers of $\log(T_{\rm eff})$, $\log g$, [Fe/H] and $f(\sigma)$ (a function of the rotational broadening parameterized by σ, the standard deviation of a Gaussian). Three sets of polynomials are defined for three temperature ranges (roughly matching OBA, FGK, and M types) with important overlap between each other where they are linearly interpolated. For the FGK and M polynomials, 26 terms are adopted; for OBA, 19 terms are used. The coefficients of these polynomials were fitted over the $\sim$2000 spectra of the library, and the choice of the terms of the $T_{\rm eff}$ limits and of weights were fine tuned to minimize the residuals between the observations and the interpolated spectra. The interpolator based on the latest ELODIE library (version 3.2) provides valid inverted atmospheric parameters covering 3100$\sim$59 000 K in $T_{\rm eff}$, 0.00$\sim$5.00 dex in $\log g$, and -2.80 $\sim$1.00 dex in [Fe/H], with the parameter space coverages shown in Fig. 2 (Prugniel et al. 2011b in preparation).

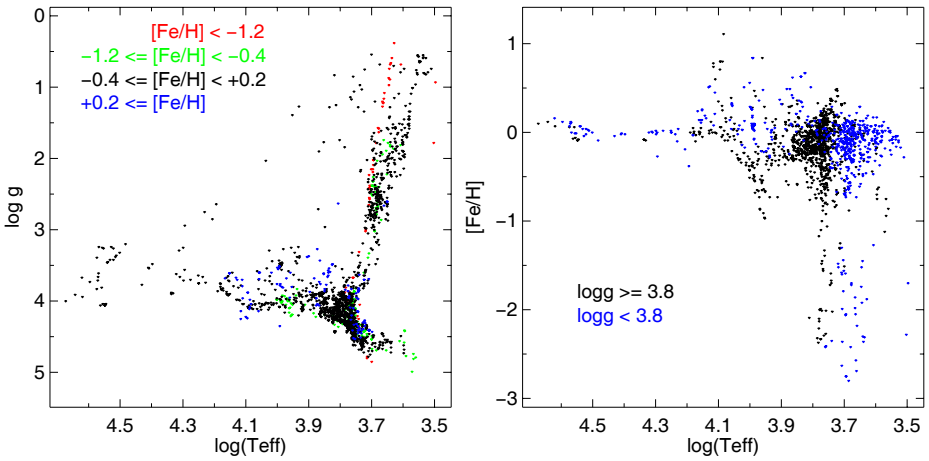

Fig. 2 Distribution of the ELODIE (version 3.2) interpolator inverted atmospheric parameters in the $\log(T_{\rm eff})$–$\log g$ plane (*left*), and in the $\log(T_{\rm eff})$–[Fe/H] plane (*right*). In the left plot, the color of the symbols distinguishes different metallicity classes. On the right, the dwarfs are shown in black and the giants in blue (color online).

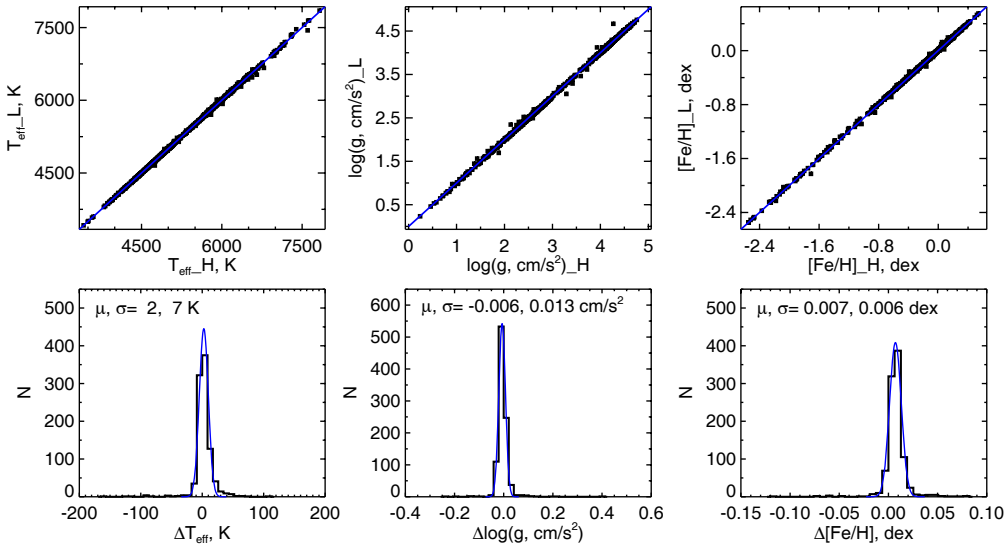

Fig. 3 Comparison of the CFLIB library's 958 F, G and K type stars' ULySS determined atmospheric parameters, between fitting the original CFLIB observations (R ∼5000, upper panels' abscissas) and those after decreasing the resolution to the same level of the LAMOST (R ∼2000, upper panels' ordinates). The blue solid lines in the upper panels are the one-to-one ratios. The histograms of the discrepancies between the two series (ordinate values minus abscissa values) are shown in the lower panels, with a fitted Gaussian in thinner blue lines which are overplotted. The offset and 1 σ standard deviation for each parameter between the two series are listed in the lower panels respectively.

3.2 Validation

In the ULySS TGM case, the model generated based on the ELODIE library[5] has FWHM = 0.58 Å, $R \sim$10 000. When ULySS performs the fitting, the model is adjusted to the same resolution and sampling as the input observation. Since ULySS has never been used to fit spectra at a resolution as low as that of LAMOST spectra, i.e., $R =$2000, we tested the effect of lower resolutions as well as different SNRs by using the CFLIB library[6] and some SDSS/SEGUE[7] spectra.

3.2.1 Validation with the Coudé-feed stellar spectral library

The CFLIB library (Valdes et al. 2004) contains 1273 stars obtained using the 0.9m coudé feed telescope at Kitt Peak National Observatory; it has a wide wavelength coverage from 3460–9464 Å, and a resolving power of $R \sim$5000 (FWHM$\sim$1.2Å). This sample of 1273 stars was selected to cover a broad regime of the three atmospheric parameters ($T_{\rm eff}$, $\log g$ and [Fe/H]), as well as the spectral type. In Wu et al. (2011), ULySS was used to homogeneously measure the atmospheric parameters for this library, and the determinations were extensively compared with the results from many other previous studies based on high resolution spectra and traditional estimation methods. For the 958 F, G, and K type stars of this library, the precision of determination for $T_{\rm eff}$, $\log g$ and [Fe/H] were 43 K, 0.13 dex and 0.05 dex respectively, and no significant systematic biases were found for the three parameters.

To test the effect of the lower resolution, we degraded the CFLIB spectra to match the resolving power of the LAMOST observations (resampling the original CFLIB spectra to 36 $\rm km\ s^{-1}$ per pixel on a logarithmic scale), and the determined atmospheric parameters were then compared with those published in Wu et al. (2011). The results are presented in Figure 3. It is shown that for $T_{\rm eff}$, $\log g$, and [Fe/H], the offsets are not significant (3 K, –0.006 dex and 0.007 dex respectively); the 1σ scatters are also negligible (7 K, 0.013 dex and 0.006 dex respectively). This demonstrates that the sacrifice in resolution of the input observation, as low as $R \sim$2000, will not affect the final accuracy of the derived atmospheric parameters, hence we can trust the results and apply ULySS to the LAMOST observations.

3.2.2 Validation with SDSS spectra: high resolution spectra and the SNR test

Since the SDSS spectroscopic survey has a similar resolving power of $R \sim$2000, it provides an ideal dataset for simulation tests on LAMOST data.

The SDSS has provided estimations of the atmospheric parameters for a subset of their observed stellar spectra since the sixth public data release (DR6, Adelman-McCarthy et al. 2008). The program to determine atmospheric parameters ($T_{\rm eff}$, $\log g$ and [Fe/H]) for SDSS/SEGUE spectra is called SSPP (Lee et al. 2008a,b), which is integrated by multiple techniques, based on medium-resolution spectroscopy and $ugriz$ photometry obtained during the course of SDSS-I and SDSS-II/SEGUE. Note that SSPP is only valid over the temperature range 4500 – 7500 K, and Lee et al. (2008a) stated the typical (external) uncertainties as $\sigma(T_{\rm eff})$ = 157 K, $\sigma(\log g)$ = 0.29 dex, and σ([Fe/H]) = 0.24 dex. Since these reported errors are computed with SDSS spectra with SNR > 50, the real uncertainties of their estimated parameters could become larger with declining SNRs (as shown in table 6 of Lee et al. 2008a). Allende Prieto et al. (2008) reported high resolution spectroscopy of 126 field stars previously observed as part of the SDSS/SEGUE. Using these calibration stars, they compared the SSPP determined parameters with those derived directly from high resolution spectra of the same stars.

[5] *http://www.obs.u-bordeaux1.fr /m2a/soubiran/elodie_library.html*

[6] *http://www.noao.edu/cflib/*

[7] *http://www.sdss.org/segue/*

To assess the reliability and precision of our determinations of the atmospheric parameters, we will fit the SDSS spectra of the high resolution (HR) templates as well as those of randomly selected samples of SEGUE stars in three different SNR ranges. We will compare the results with the HR (Allende Prieto et al. 2008) and SSPP measurements.

1) *Validation from the SDSS High-Resolution Spectroscopy: High Resolution Test*

Out of the 126 SDSS stars with stellar atmospheric parameters measured from high resolution spectra listed in Allende Prieto et al. (2008), we selected 125, excluding SDSS J205025.83–011103.8 for which SSPP failed to fit. The high resolution spectra were obtained by Keck I/HIRES (Vogt et al. 1994), Keck II/ESI (Sheinis et al. 2002), VLT/UVES, HET/HRS (Ramsey et al. 1998; Tull 1998), and SUBARU/HDS (Noguchi et al. 2002); details about the methods for determining the parameters of these different spectra are described in Allende Prieto et al. (2008). They empirically determined the typical random uncertainties of the $T_{\rm eff}$, $\log g$, and [Fe/H] delivered by the SSPP to be 130 K (2.2 %), 0.21 dex, and 0.11 dex respectively. They then compared SSPP estimations and those measurements derived from the high resolution spectra of SDSS stars. When comparing with the HET data sample which contains 81 stars, the standard deviation of the differences are 2.75%, 0.25 dex and 0.12 dex for $T_{\rm eff}$, $\log g$ and [Fe/H] respectively, but when comparing with data of the other sources (e.g., Keck, SUBARU), the 1σ errors are 3.14%, 0.46 dex and 0.41 dex respectively, as listed in table 6 of Allende Prieto et al. (2008).

Here we made the following comparisons:

(1) Parameters given by SSPP with the ones derived from the SDSS HR data;
(2) ULySS determined parameters (fitting the SDSS/SEGUE survey spectra) with those derived from the SDSS HR data;
(3) ULySS determined parameters with the ones given by SSPP.

Results are sequentially displayed in Figures 4, 5, 6, and Table 2. Unlike Allende Prieto et al. (2008), our comparison between SSPP and HR measurements, as listed in the top row of Table 2, are averaged values. It is found that the SSPP estimated temperatures are systematically 120 K higher than the HR results; this feature is comparable with the results specified in Allende Prieto et al. (2008), where they stated that for the HET sample (number = 81), SSPP indicated higher $T_{\rm eff}$ by about 170 K ($\sim$3.11%), and for the other data sample (Keck & SUBARU, number = 44), the bias in $T_{\rm eff}$ is $\sim$–0.58% (in their sect. 6.2 and table 6).

Figure 5 shows that there is no notable offset between the ULySS determined $T_{\rm eff}$ and that measured from HR spectra. Thus not surprisingly, there is a 109 K systematic difference between the ULySS and SSPP temperatures as shown in Table 1 and Figure 6. There is no obvious systematic differences in $\log g$ among the three measurements. As for the metallicity, SSPP measurements are a little bit lower than the HR results, but the ULySS estimations are somewhat higher than the HR values, with an offset of 0.13 dex between the ULySS and SSPP values. For the 1σ errors of the three atmospheric parameters, both ULySS and SSPP estimations are in an acceptable range, as shown by comparing with parameters derived from the HR data, and the ULySS and SSPP values are quite consistent with each other. This is not unexpected, since both of these methods are processing medium-resolution spectra in an automated way, which would result in measurements with more or less similar uncertainties.

2) *Validation with SEGUE SSPP Determinations: the SNR Test*

For the purpose of validation and calibration of the SSPP output, only bright stars in the SDSS/SEGUE sample were accessible for follow-up high resolution spectroscopic observations, thus the available SDSS high resolution spectra have quite high SNR, e.g. with SNR = $20 \sim 80$ as indicated in table 1 of Allende Prieto et al. (2008). However, most of the SDSS stellar spectra have significantly lower SNRs, typically $10 \sim 20$ wavelength-averaged values (sect. 7 of Allende Prieto

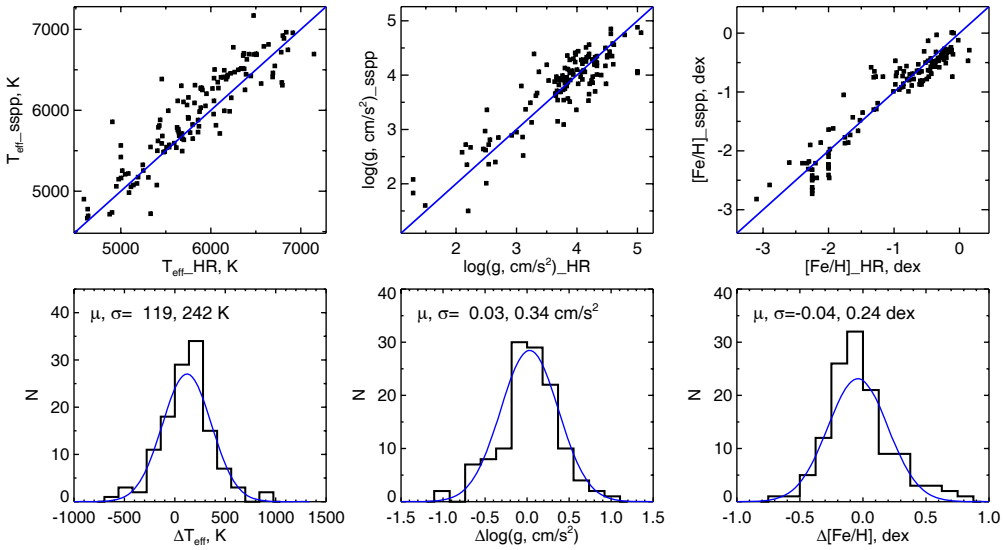

Fig. 4 Comparison of the SSPP determined atmospheric parameters with those derived from the SDSS high resolution spectra for 125 SDSS observations. The convention is the same as in Fig. 3.

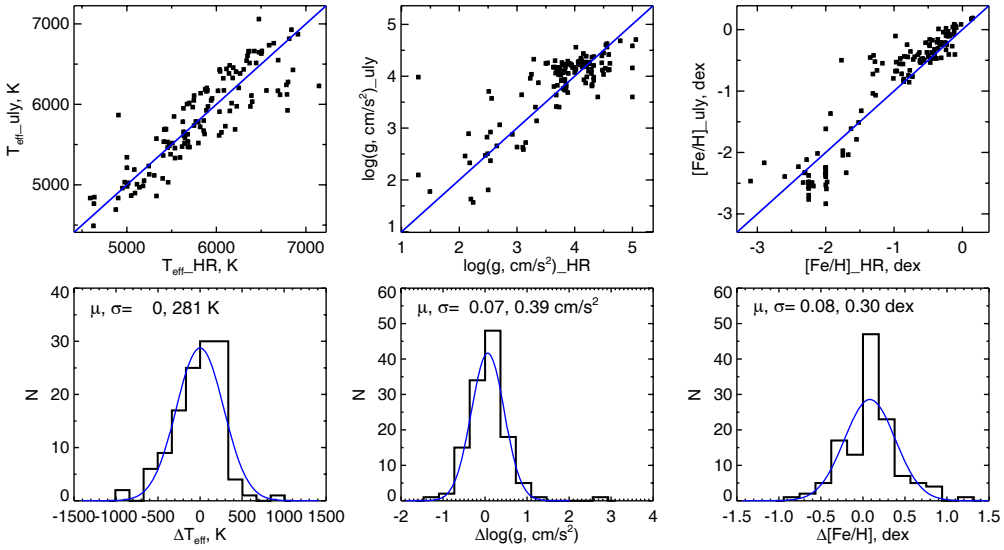

Fig. 5 Comparison of the ULySS determined atmospheric parameters (fitting the SDSS/SEGUE survey spectra) with those derived from the SDSS high resolution spectra for 125 SDSS observations. The convention is the same as in Fig. 3.

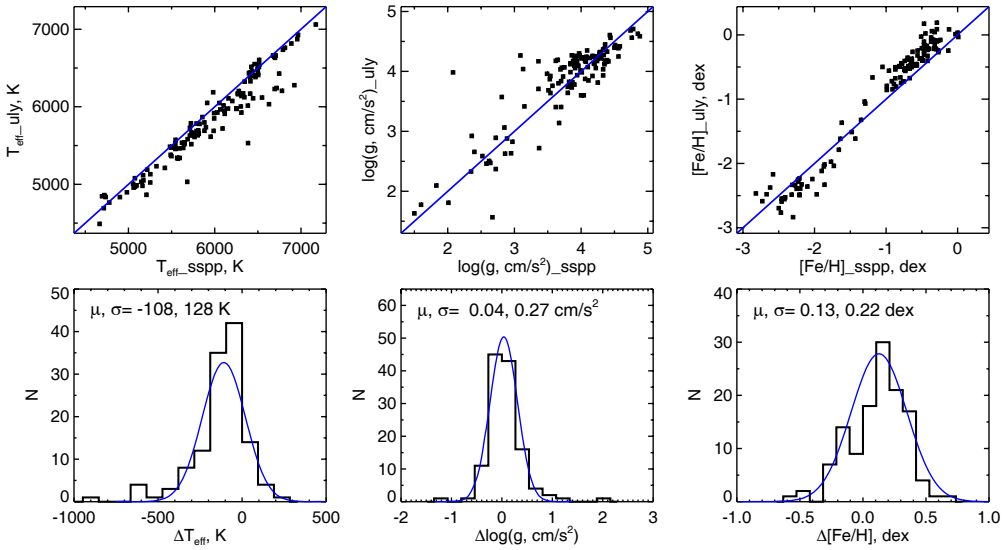

Fig. 6 Comparison of the ULySS determined atmospheric parameters with those given by SSPP for 125 SDSS observations. The convention is the same as in Fig. 3.

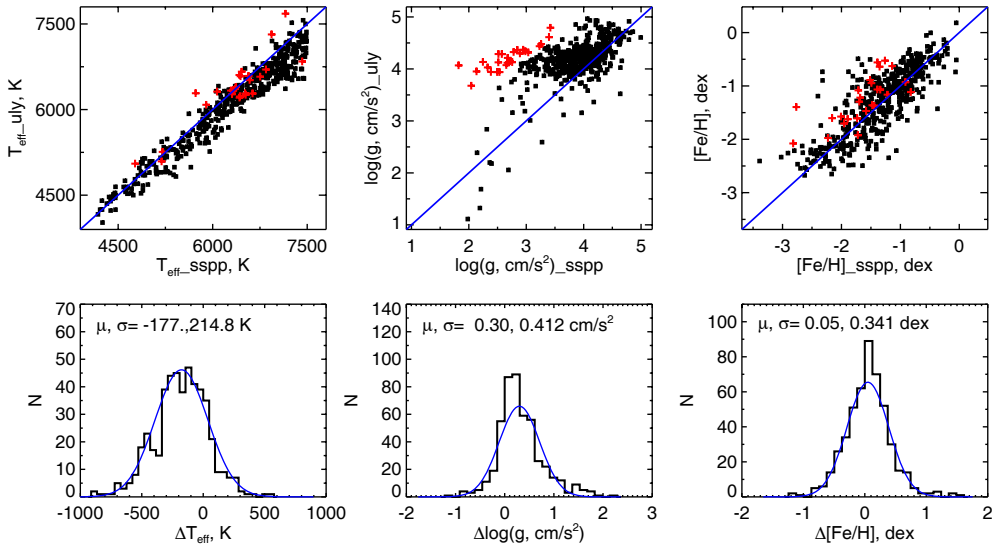

Fig. 7 Comparison of the ULySS determined atmospheric parameters with those computed by the SEGUE SSPP for 486 randomly selected SDSS observations with SNR between 10 and 20. There are 26 (out of 486) discrepant $\log g$ measurements; they are displayed in red crosses (color online) and discussed in the text. The convention is the same as in Fig. 3.

Table 2 Comparisons between the Atmospheric Parameters Derived from the SDSS High Resolution Spectra with those determined by ULySS and SSPP for 125 objects.

Comparison	$\Delta T_{\rm eff}$ (K)		$\Delta \log g$ (cm s^{-2})		Δ[Fe/H] (dex)	
	μ	σ	μ	σ	μ	σ
SSPP vs. HR	120	243	0.03	0.34	–0.04	0.24
ULySS vs. HR	0	282	0.07	0.39	0.08	0.30
ULySS vs. SSPP	–109	129	0.04	0.27	0.13	0.22

Notes: The μ & σ are computed by the former one minus the latter one, e.g., for the first line, they are the values of ULySS–HR parameters.

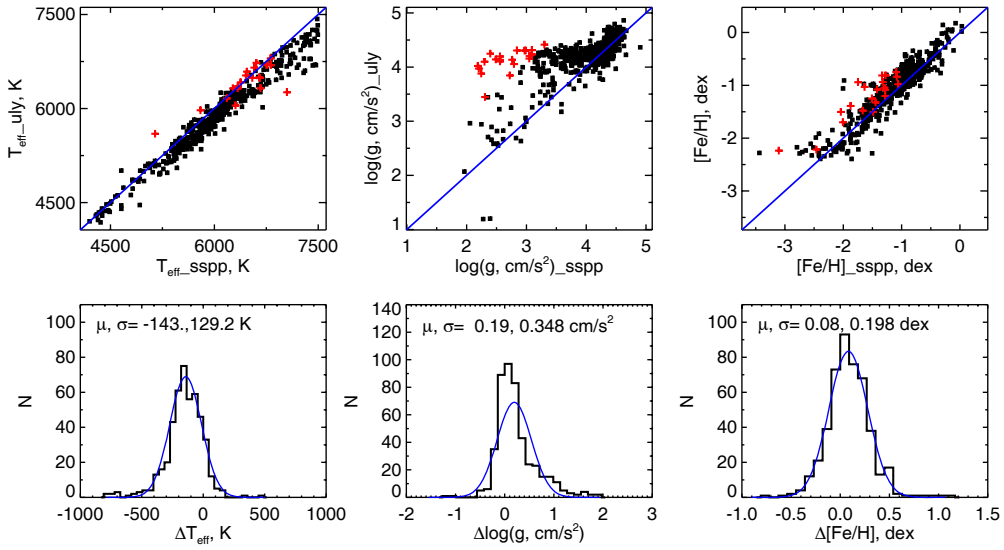

Fig. 8 Comparison of the ULySS determined atmospheric parameters with those computed by the SEGUE SSPP for 466 randomly selected SDSS observations with SRN between 20 and 30. There are 21 (out of 466) $\log g$ discrepant measurements; they are displayed in red crosses (color online) and discussed in the text. The convention is the same as in Fig. 3.

et al. 2008). By using the SEGUE sample data, we have checked the impact of different SNRs on the ULySS determined atmospheric parameters.

We randomly selected some SEGUE spectra together with the related SSPP estimates for which all the three atmospheric parameters were available. As mentioned in Lee et al. (2008a), the SSPP is reliable in the temperature region cooler than 7500 K, so we picked the data with this $T_{\rm eff}$ upper restriction. We divided them into three groups, with SNRs in the region of $10 \sim 20$, $20 \sim 30$ and > 30. Each group contains around 475 spectra, mostly F, G, and K type stars. The statistics of all the three groups' comparisons are shown in Table 3. The comparisons between the ULySS estimated stellar atmospheric parameters and those from the SSPP at different SNR regions are displayed sequentially in Figure 7, Figure 8, and Figure 9.

For the three parameters, the mean offsets and the 1σ errors of the third group are equivalent to the previous comparison results between ULySS and SSPP (see Table 2). Consistently, we can see that the SSPP determined $T_{\rm eff}$ were underestimated by more than 100 K when compared to the ULySS results. The estimation precision of the $\log g$ is to some extent lower than the $T_{\rm eff}$ and

Table 3 Comparisons of the ULySS Determined Atmospheric Parameters with Those Computed by SEGUE SSPP for Some Randomly Selected SDSS Survery Observations with Different SNR.

SNR Group	Num.	$\Delta T_{\rm eff}$ (K)		$\Delta \log g$ (cm s^{-2})		Δ[Fe/H] (dex)	
		μ	σ	μ	σ	μ	σ
$10 \sim 20$	486	–177	214.8	0.30	0.412	0.05	0.341
	460	–186	208.9	0.26	0.357	0.03	0.332
$20 \sim 30$	466	–143	129.2	0.19	0.348	0.08	0.198
	445	–147	125.3	0.17	0.308	0.07	0.191
> 30	476	–133	87.9	0.07	0.215	0.09	0.142
	465	–134	85.5	0.07	0.211	0.09	0.140

Notes: The μ & σ were computed by the ULySS estimations minus the SSPP measurements. For each comparison group, the first line gives the raw statistics, while the second line gives the statistics after excluding the $\log g$ outliers which are shown in red crosses in Fig. 7, Fig. 8, and Fig. 9, respectively.

[Fe/H]. From Figures 7, 8, and 9, in each figure's $\log g$ panel (upper middle one), there exists a strange stripe in the region of $\log g < 3.50$ dex, where the SSPP determined $\log g$ are systematically smaller than the ULySS ones. We marked those discrepant values, with a $\log g$ difference greater than 0.90 dex, as red crosses in the three comparison figures. The statistics after excluding the discrepant measurements are listed in each group's second line in Table 3.

We searched for the cause of the discrepancies by checking the differences between the SSPP determinations and those derived from the SDSS/SEGUE high resolution spectra; the result is shown in Figure 10. This figure is a contour map of the differences of the surface gravity (SSPP minus HR), while the X and Y axes are the $T_{\rm eff}$ and [Fe/H] values from the high resolution spectra. Apparently, in the region of $T_{\rm eff}$ above 6300 K, the SSPP determined surface gravities are systematically underestimated by about 0.4 dex (on average), and this region (blue basin) spreads widely in the [Fe/H] space. In the solar-like metallicity region, the $\log g$ difference could become as big as –0.60 dex, and the bias area can extend to $T_{\rm eff}$ =5000 K. In the metal-poor area around [Fe/H] = –2.30 dex and $T_{\rm eff}$ = 6500 K, the $\log g$ difference can also be as big as –0.60 dex. Comparing to our detected $\log g$ deviations shown in Figure 7 $\sim$ Figure 9's temperature panels, those red crosses are likely associated with and reside in the blue basin shown in Figure 10; most of them occupy the temperature region above 6300 K, and are distributed loosely over the metallicity panel. With this investigation, the $\log g$ deviations detected in our comparisons between the ULySS and SSPP's solutions seem to some extent coming from the internal bias of the SSPP pipeline in a specific parameter space — the area of the $\log g$ differences are presented in the blue basin shown in Figure 10's right part. This blue basin's mean bias is about 0.40 dex, and we defined the red crosses as deviations with $\log g$ difference > 0.90 dex; the magnitudes of the difference are not exact matches. The contour map is only prepared by using 125 SDSS/SEGUE high resolution bright calibration stars (SNR between $20 \sim 80$). For the majority of the SDSS/SEGUE fainter survey spectra with much lower SNR ($10 \sim 20$), the bias area — the blue basin, is possibly becoming worse (see statistical examples shown in table 6 of Lee et al. 2008a). We cannot give any firm conclusion about the origin of the biases, but we cannot exclude that they are due to SSPP. This bias affects 4% of the sample that we studied, and we can consider our determinations as reasonably reliable.

Our tests also show that the precision is decreasing as the SNR declines, but the determinations do not appear to be biased.

4 DETERMINING ATMOSPHERIC PARAMETERS OF LAMOST STARS USING ULYSS

4.1 Determining Strategy for ULySS based on the LAMOST Observations

We established above that we can get reliable measurements of the atmospheric parameters from LAMOST spectra using ULySS. Since the model is based on the ELODIE library with a wavelength

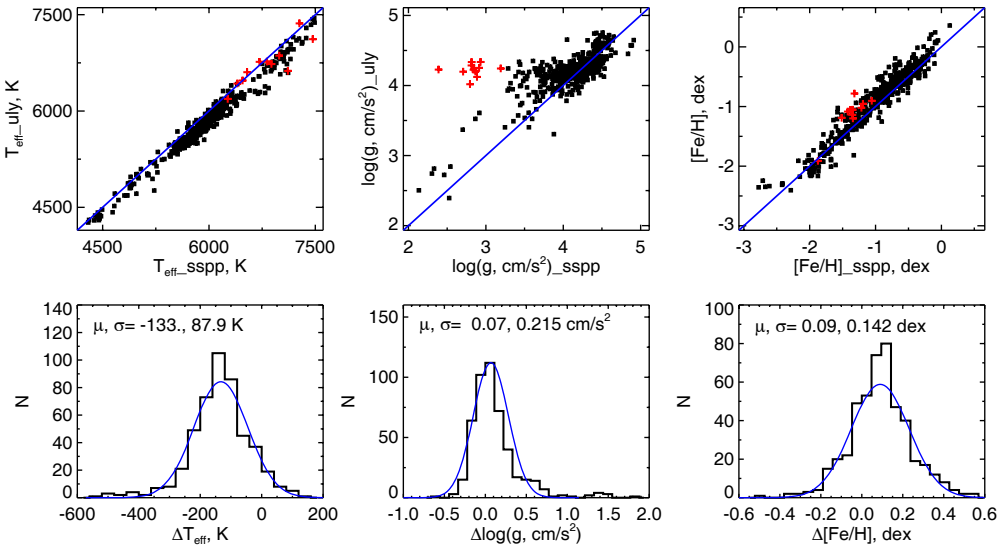

Fig. 9 Comparison of the ULySS determined atmospheric parameters with those computed by the SEGUE SSPP for 476 randomly selected SDSS observations with SNR greater than 30. There are 11 (out of 476) $\log g$ discrepant measurements; they are displayed in red crosses and discussed in the text. The convention is the same as in Fig. 3.

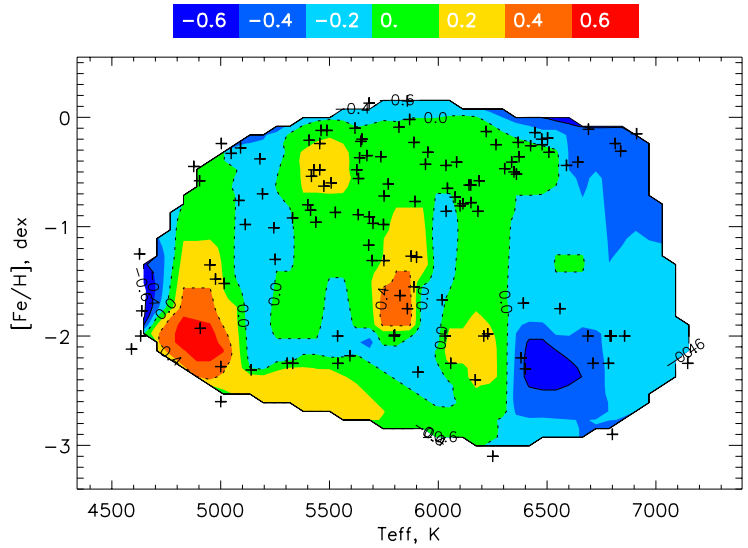

Fig. 10 Contour map of the differences between the SSPP determined $\log g$ and those values derived from the SDSS/SEGUE high resolution stellar spectra. The X and Y axes are the effective temperature and metallicity values derived from the high resolution spectra. The black crosses present the positions where there exist actual spectral data.

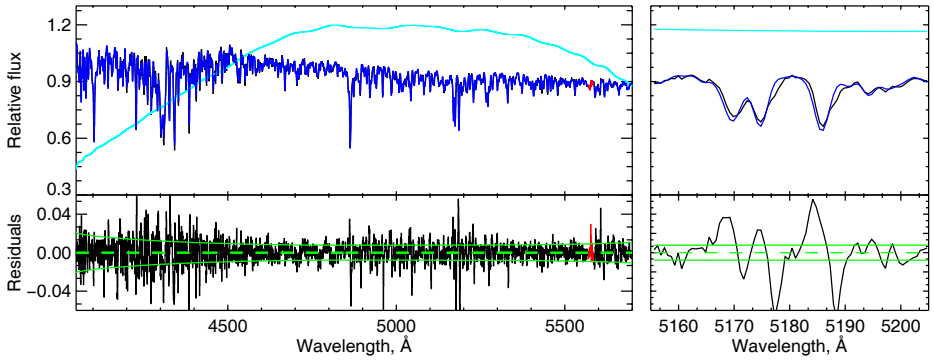

Fig. 11 ULySS fit of LAMOST observation, obtained with spectrograph no. = 4, and fiber no. = 193, with a TGM component. The top panel shows the spectrum (in black) and the best fit (in blue, both are almost superimposed and the black line can only be seen when zooming in on the figure); the light blue is the multiplicative polynomial. In red, we plot the flagged and masked NaD telluric lines which were not well calibrated in the ELODIE library. The residuals are plotted in the bottom panels. The continuous green lines mark the 1-σ deviation, and the dashed line is the zero-axis. The right side expands to a wavelength range around Mg_b.

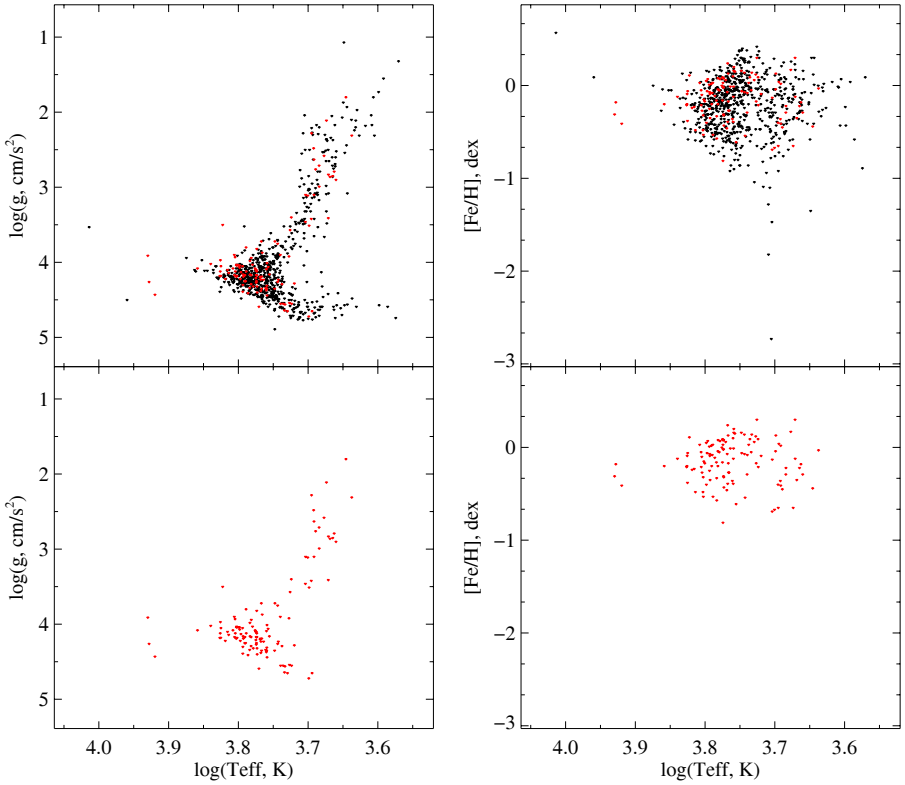

Fig. 12 Distribution in the $\log(T_{\rm eff})$–$\log g$ planes (*left*) and in the $\log(T_{\rm eff})$–[Fe/H] planes (*right*) of the adopted atmospheric parameters for the 771 LAMOST observed stars. The 120 red points present the selected empirical templates for the LAMOST. For clarity, they are separately displayed in the bottom panels.

coverage between 3900 Å and 6800 Å, we will only use the blue arm of the LAMOST. Since the method does not require the spectra to be flux-calibrated, we can use the present commissioning data.

ULySS executes a local minimization procedure. When approaching a new data set with new coverage of wavelength, resolution, parameters, etc., one should use the ULySS software-package convergence map tool to study the structure of the parameter space and find the region where the local minima can potentially trap the solution; see examples in Wu et al. (2011) and Koleva et al. (2009a). For this work, since the targets are relatively bright stars, we chose the starting guess grids for the three parameters as $T_{\rm eff}$ =[4000, 7000, 15 000] K, $\log g$ =[1.8, 3.8] dex, and [Fe/H] = [–1, 0] dex. The final solution (absolute minimum) is the best from those obtained with different guesses.

Although the blue arm of LAMOST covers wavelengths 3700∼5900 Å, due to the low instrumental response in the red, we exclude the data above 5700 Å. Moreover, since the ELODIE spectra's SNR drops in the blue end, we restricted our fit range to be in 4050∼5700 Å. During the fitting procedure, gaps, bad pixels, etc., are automatically rejected by the kappa-sigma clips.

To estimate the errors, normally we need to know the random errors of each wavelength element. Unfortunately, since the LAMOST 2D pipeline is still in an early stage of development, it could not provide reliable errors for this. Thus, following Wu et al. (2011), we simply determined an upper limit for these internal errors by assuming that the residuals purely come from the noise, i.e. the fit is perfect. With this hypothesis, the reduced χ^2 is by definition equal to unity. To make this determination, we assumed that the noise was the same at all wavelength points, and performed the fit with an arbitrary value of SNR and re-scaled the errors returned by ULySS by multiplying them by $\sqrt{\chi^2}$. To estimate the external errors, we multiplied the internal errors by a coefficient computed to match the comparisons made with SDSS/SEGUE (statistics listed in Table 2), and assuming that the uncertainties are similar for both series.

4.2 ULySS Determined Atmospheric Parameters

For the selected 771 LAMOST stellar spectra from the commissioning database, we determined their atmospheric parameters by using the ULySS package. All the estimates are presented in Table 1 (five objects are shown; the full table is available in the electronic version), with typical mean internal error bars of 39 K, 0.21 dex and 0.11 dex for $T_{\rm eff}$, $\log g$ and [Fe/H] respectively. An example of the ULySS fit displayed in Figure 11 illustrates the general quality. The distribution of all the ULySS determined atmospheric parameters for our LAMOST data sample is shown in Figure 12. Clearly, all the solutions are located in the valid estimated parameter space region as shown in Figure 2 of the ELODIE library (version 3.2). From these results, although there are eight metal-poor star candidates (with [Fe/H] < -1.0 dex), most of our selected stars cluster around the metal-rich region. This phenomenon is restricted by the availability of the LAMOST commissioning data set, since the commissioning work is continuing. In the near future, we will collect and investigate more stars with various metallicites.

4.3 Comparison with Atmospheric Parameters Determined by the SSPP

For an auxiliary check, we compared our determined atmospheric parameters with those derived by SSPP (version 7.5 via private communication with T.C. Beers). ULySS determination is fitted within the wavelength range of 4050–5700 Å, but the SSPP requires the input spectra to cover the whole wavelength range in 3800∼9200 Å. Therefore, we combined the blue and red arm spectra. Before this step, we visually selected several F8 type stars in our sample for each spectrograph, and used them to correct the flux for both the blue and red arm data. Excluding those targets with missing red arm spectra or with low SNR, 559 out of 771 selected objects were processed with the SSPP.

The measurements of these 559 objects are compared in Figure 13 with mean biases (-223 K, -0.17 dex, 0.03 dex) and 1σ errors (167 K, 0.34 dex, 0.16 dex) listed on the bottom panels for each parameter. The -223 K systematic bias of the $T_{\rm eff}$ is consistent with our previous validation result for low SNR spectra. In the surface gravity panel of Figure 13, there is a substructure in the region of $\log g < 3.9$ dex. There the ULySS measurements are systematically underestimated by about 0.6 dex (on average) when compared to the SSPP determinations. In Wu et al. (2011), for the CFLIB library's 958 F, G and K type stars, ULySS could reach a precision in $\log g$ of 0.13 dex with no significant bias. The work of Smolinski et al. (2011) could somewhat help us answer this problem. This paper is actually one of the series of papers coming after Lee et al. (2008a,b) and Allende Prieto et al. (2008). They increased the number of SDSS/SEGUE high resolution stellar spectra by including an extended sample of Galactic globular and open cluster member stars. In addition, they announced recent modifications in the SSPP pipeline (mainly improving their methods for the determination of the [Fe/H] and the radial velocity, for the $T_{\rm eff}$ and $\log g$ there is not much change) and it has been updated from version 7 to version 8. The new version 8 has been applied to the SDSS Data Release 8 (DR8) which was scheduled for Dec. 2010. By using their high resolution calibration stars, they made surface gravity comparison between the SSPP determinations and those values derived from the high resolution spectra for both SSPP version 7 and 8. Their comparison results are displayed in Figure 14; version 7 results are shown in black while version 8's are shown in red. Figure 14 clearly shows that when $\log g$ is less than 3.9 dex, on average, the SSPP estimations are overestimated by ~ 0.6 dex when compared to the high resolution spectral derivations. This phenomenon explains why there is a substructure found in Figure 13's $\log g$ panel. The problem is mostly related to the SSPP not functioning optimally in this specific $\log g$ region.

The problem shown in this section is different from that found in Figures 7, 8, and 9 (Section about the SNR Test), and these two kinds of inconsistent cases do not conflict with each other. The $\log g$ problem discussed in the previous context is for stars with effective temperature above 6300 K, and can affect about 4% of the data sample. In the $\log g$ panel of Figure 13 we can see several stars that appear in that bias region. The problem shown in this section is actually tending toward giants. No apparent visible substructure bias feature could be found in Figures 7–9, because in that randomly selected data sample, only a few giants are included.

For the metallicity, our comparison does not show significant bias. For the 1σ errors of the three parameters, they are in good agreement with our validation results listed in Table 3. The dispersion in $\log g$ is bigger than the other two parameters, though, as mentioned before, $\log g$ is the hardest to estimate because of the low resolution spectral survey data. Here its larger dispersion may be partially due to the low quality of LAMOST commissioning spectra, i.e., the low SNR, poor flux-calibration and simple connection with the blue and red arms, that lead to the SSPP's failure in measuring some of our selected spectra. Furthermore, we should keep in mind that the SSPP is purposefully tailored and adjusted based on SDSS/SEGUE spectra rather than LAMOST observations. The spectra observed by SDSS/SEGUE and LAMOST are different, and have their own intrinsic characteristics related with each independent telescope design, instrumentation and observational conditions. We would expect the subset offset and large dispersion in surface gravity determination to be reduced by both improving the SSPP and ULySS capability in the determination of the stellar atmospheric parameters, as well as the quality of the input LAMOST spectral data. Here our comparison shows that the two series of the derived parameters are consistent with each other on an acceptable scale for spectroscopic observations at medium-resolution ($R \sim$2000).

5 BUILDING THE STELLAR SPECTRA TEMPLATES FOR LAMOST

Our task is aimed at building an empirical set of stellar spectral templates for LAMOST, and at present, we have selected 771 LAMOST observed targets. LAMOST practically covers the wavelength range of 3700–9000 Å, but since the flux calibration was not sufficiently reliable and thus

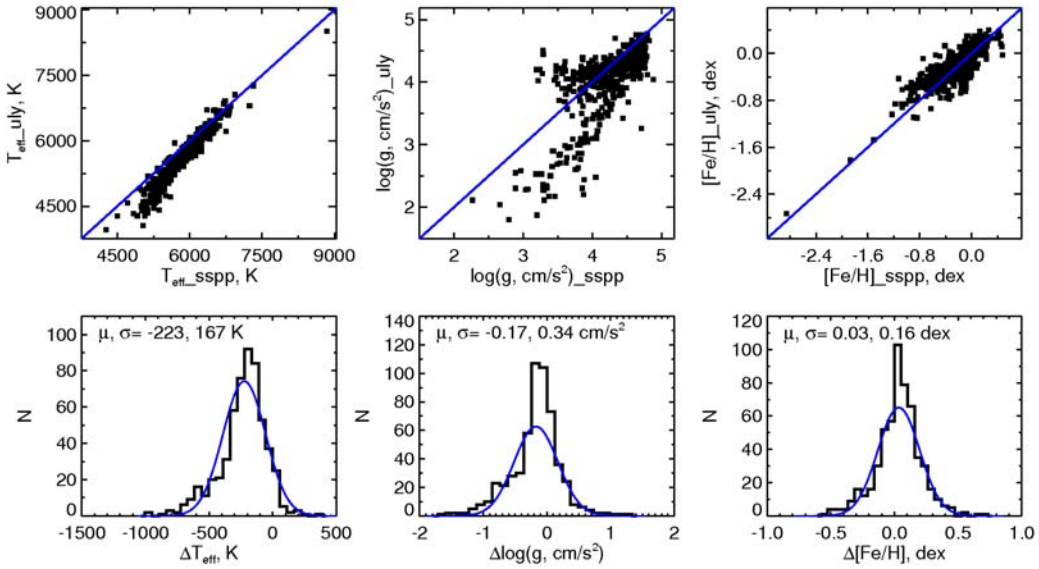

Fig. 13 Comparison of the ULySS determined atmospheric parameters with those from SSPP for 559 selected LAMOST observations. The convention is the same as in Figure 3.

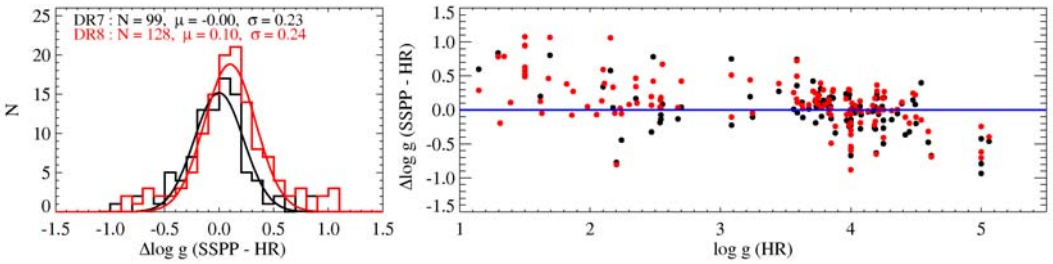

Fig. 14 Surface gravity comparison between the SSPP version 7 and the SSPP version 8 for the high-resolution calibration stars. The red dots (color online) and lines are associated with the SSPP version 8, while the black dots and lines correspond to the SSPP version 7. This figure is adopted from figure A1 of Smolinski et al. (2011).

not performed on the spectra, the blue and red arm spectra were separated. However, for the template library, it is preferred that the template spectra cover the full wavelength range. As described in Section 4.3, we adopted a coarse method to correct the flux and then combined the blue and red arm spectra. Because of the low quality of the LAMOST commissioning data, and the uncertainties of the flux calibration and the spectral combinations, we selected template spectra by careful visual inspection, together with consideration of the atmospheric parameter coverage. Finally, out of 771 targets, 120 with relatively good quality were chosen as basic ingredients to build a primary version of the LAMOST stellar spectral template library. These objects are displayed in red dots in Figure 12 (in both upper and lower panels) and listed in Table 1 (Flag = 1), with parameters covering the stellar

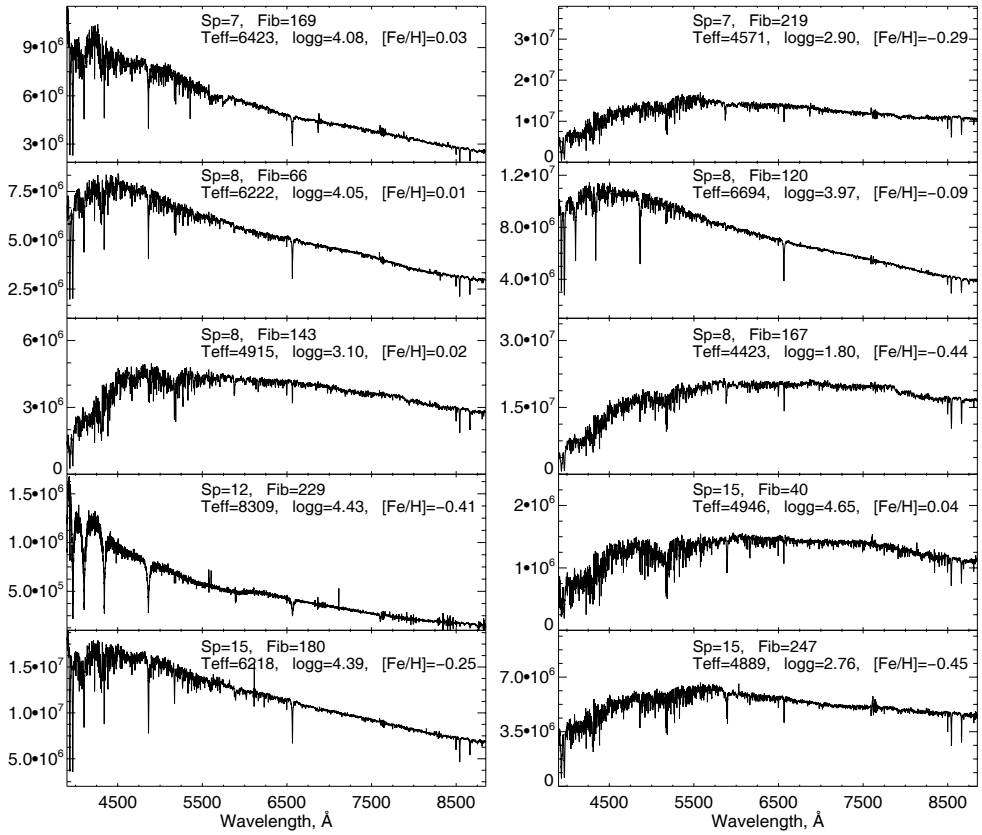

Fig. 15 Examples of 10 selected empirical stellar spectral templates of LAMOST stars. These spectra have rough flux-calibration and non pseudo continuum subtraction. The relative fluxes are in units of the original counts per pixel. 'Sp' is the spectrograph number; 'Fib' is the fiber ID number.

parameter space of 4339∼8507 K in $T_{\rm eff}$, 1.80∼4.72 dex in $\log g$, and $-0.81 \sim 0.30$ dex in [Fe/H] respectively. Most of them are F, G, and K dwarfs. To illustrate them in more detail, 10 of the sample template spectra are shown in Figure 15. We hereby define this newly built LAMOST stellar spectral template library to be Version 1.0.

6 SUMMARY AND PROSPECTS

One of the goals of LAMOST surveys will be to explore the intrinsic properties of stars in the Milky Way. To address this, we examine the precision of the three fundamental stellar atmospheric parameters ($T_{\rm eff}$, $\log g$ and [Fe/H]) that could be derived from the LAMOST commissioning observations.

After various validation tests, we demonstrated that ULySS is an effective tool for measuring large stellar survey spectra at medium-resolution ($R \sim$2000). For the first time, we have shown that this method can determine the three principal stellar atmospheric parameters ($T_{\rm eff}$, $\log g$ and [Fe/H]) based on LAMOST stellar spectra to an accuracy comparable to (or maybe better than) that of other measurement approaches like the SSPP. The imbedded multiplicative polynomial in ULySS, which is used to absorb errors in the flux calibration, helps bypass the step of normalization to the pseudo-

continuum which is usually required by other methods. This feature of ULySS is especially favorable for LAMOST commissioning data, as the flux-calibration has not yet been performed.

We selected 771 stars from the LAMOST commissioning data with spectra of relatively good quality. We measured their parameters with precisions of 167 K, 0.34 dex and 0.16 dex for $T_{\rm eff}$, $\log g$ and [Fe/H] respectively.

This provides us with a good opportunity to construct an empirical stellar spectral template library for LAMOST. At present, this first version consists of 120 stars (the best of the 771 selected above). This stellar spectral template library for LAMOST is valuable and reliable, and it will be used as a standard reference frame customized for the LAMOST to measure the stellar atmospheric parameters using various methods. The library will be upgraded in the future, aiming at

- Enlarging the LAMOST stellar spectral template library. LAMOST will continue its commissioning observation, targeting a number of open and globular clusters, as well as many bright field stars, and it is possible to obtain larger data sets for tests and selections. We plan to include more samples in the higher and lower temperature regions with different metallicities. The final goal will be to produce an empirical LAMOST stellar spectral template library that contains several hundred members with wide coverage in the atmospheric parameter space.
- Assignment of the spectral classifications of the template stars. To construct a template library, it would be more helpful to include the spectral type of the template star. We plan to add approximate MK spectral classification for our empirical template stars. Methods in Singh et al. (1998); Bailer-Jones (2002); Hawley et al. (2002); Covey et al. (2007) and Bazarghan & Gupta (2008) may be adopted if they could provide reliable results for LAMOST observations (Wu et al. in preparation).
- As described in Section 2, LAMOST is still in its commissioning period, with problems in the data reduction pipeline, e.g., sky-subtraction, flux-calibration, etc., that still need to be solved. With the ongoing adjustments of the instrument and software, we believe that the quality of the LAMOST data will be greatly improved and the templates will be updated accordingly.

The newly built LAMOST stellar spectral template library (version 1.0) can be readily deployed in the automated 1D parametrization pipeline of LAMOST. The quality of the template directly relies on an accurate calibration and pre-processing of the spectra. Since the LAMOST commissioning period is still ongoing, future versions of the template library will be constructed based on the availability of the improved and enlarged LAMOST observational database.

Overall, we first effectively determine the stellar atmospheric parameters ($T_{\rm eff}$, $\log g$ and [Fe/H]) of the LAMOST real observations (771 homogeneously selected stars) and test the estimation precisions on each parameter with external comparisons. Moreover, based on this data sample, we select a sub-sample, and use these data in constructing a preliminary version of the LAMOST stellar spectral template library (version 1.0). This work gives us an early insight on the scientific capability of the LAMOST for the research work related to our Milky Way.

Acknowledgements The authors are grateful to the anonymous referee for valuable comments and Dr. James Wicker for amending the language of our manuscript. We would like to thank Dr. T. C. Beers for sharing the SSPP (version 7.5) with us, and Dr. Xiaoyan Chen for many useful suggestions. We thank Fengfei Wang's help on selecting F type stars (which were used in the approximate flux calibration). We acknowledge the grant supports given by the National Natural Science Foundation of China (Grant Nos. 10973021, 10778626 and 10933001), the National Basic Research Development Program of China (Grant No. 2007CB815404), and the Young Researcher Grant of National Astronomical Observatories, Chinese Academy of Sciences. Yue Wu also acknowledges support from the China Scholarship Council (CSC) (Grant No. 2007104275).

The Guoshoujing Telescope (LAMOST) is a National Major Scientific Project built by the Chinese Academy of Sciences. Funding for the project has been provided by the National

Development and Reform Commission. The LAMOST is operated and managed by the National Astronomical Observatories, Chinese Academy of Sciences. This work was made using the SDSS/SEGUE data and their CAS database[8].

Funding for the Sloan Digital Sky Survey (SDSS) and SDSS-II has been provided by the Alfred P. Sloan Foundation, the Participating Institutions, the National Science Foundation, the US Department of Energy, the National Aeronautics and Space Administration, the Japanese Monbukagakusho, the Max Planck Society, and the Higher Education Funding Council for England. The SDSS Web site is *http://www.sdss.org*. The SDSS is managed by the Astrophysical Research Consortium (ARC) for the Participating Institutions. The Participating Institutions are the American Museum of Natural History, the Astrophysical Institute Potsdam, the University of Basel, the University of Cambridge, Case Western Reserve University, the University of Chicago, Drexel University, Fermilab, the Institute for Advanced Study, the Japan Participation Group, The Johns Hopkins University, the Joint Institute for Nuclear Astrophysics, the Kavli Institute for Particle Astrophysics and Cosmology, the Korean Scientist Group, the Chinese Academy of Sciences (LAMOST), Los Alamos National Laboratory, the Max Planck Institute for Astronomy (MPIA), the Max Planck Institute for Astrophysics (MPA), New Mexico State University, Ohio State University, the University of Pittsburgh, the University of Portsmouth, Princeton University, the United States Naval Observatory, and the University of Washington.

References

Adelman-McCarthy, J. K., Agüeros, M. A., Allam, S. S., et al. 2008, ApJS, 175, 297
Allende Prieto, C., Beers, T. C., Wilhelm, R., et al. 2006, ApJ, 636, 804
Allende Prieto, C., Sivarani, T., Beers, T. C., et al. 2008, AJ, 136, 2070
Alonso, A., Arribas, S., & Martinez-Roger, C. 1996a, A&AS, 117, 227
Alonso, A., Arribas, S., & Martinez-Roger, C. 1996b, A&A, 313, 873
Alonso, A., Arribas, S., & Martínez-Roger, C. 1999a, A&AS, 139, 335
Alonso, A., Arribas, S., & Martínez-Roger, C. 1999b, A&AS, 140, 261
An, D., Johnson, J. A., Beers, T. C., et al. 2009, ApJ, 707, L64
Árnadóttir, A. S., Feltzing, S., & Lundström, I. 2010, A&A, 521, A40
Bagnulo, S., Jehin, E., Ledoux, C., et al. 2003, The Messenger, 114, 10
Bailer-Jones, C. A. L. 2000, A&A, 357, 197
Bailer-Jones, C. A. L. 2002, in Automated Data Analysis in Astronomy, eds. R. Gupta, H. P. Singh, & C. A. L. Bailer-Jones (London: Narosa Pub. House), 83
Bailer-Jones, C. A. L., Irwin, M., Gilmore, G., & von Hippel, T. 1997, MNRAS, 292, 157
Barbuy, B., Perrin, M.-N., Katz, D., et al. 2003, A&A, 404, 661
Bazarghan, M., & Gupta, R. 2008, Ap&SS, 315, 201
Beers, T. C., Rossi, S., Norris, J. E., Ryan, S. G., & Shefler, T. 1999, AJ, 117, 981
Bond, N. A., Ivezić, Ž., Sesar, B., et al. 2010, ApJ, 716, 1
Bouchard, A., Prugniel, P., Koleva, M., & Sharina, M. 2010, A&A, 513, A54
Castelli, F., & Kurucz, R. L. 2003, in Modelling of Stellar Atmospheres, IAU Symposium, vol. 210, eds. N. Piskunov, W. W. Weiss, & D. F. Gray, 20P (arXiv: astro-ph/0405087)
Cayrel, R., Perrin, M.-N., Barbuy, B., & Buser, R. 1991, A&A, 247, 108
Cenarro, A. J., Cardiel, N., Gorgas, J., et al. 2001a, MNRAS, 326, 959
Cenarro, A. J., Gorgas, J., Cardiel, N., et al. 2001b, MNRAS, 326, 981
Cenarro, A. J., Peletier, R. F., Sánchez-Blázquez, P., et al. 2007, MNRAS, 374, 664
Chen, X. Y., Liang, Y. C., Hammer, F., et al. 2010, A&A, 515, A101
Coelho, P., Barbuy, B., Meléndez, J., Schiavon, R. P., & Castilho, B. V. 2005, A&A, 443, 735

[8] *http://cas.sdss.org/*

Covey, K. R., Ivezić, Ž., Schlegel, D., et al. 2007, AJ, 134, 2398
Gustafsson, B., Edvardsson, B., Eriksson, K., et al. 2008, A&A, 486, 951
Hawley, S. L., Covey, K. R., Knapp, G. R., et al. 2002, AJ, 123, 3409
Heap, S. R., & Lindler, D. J. 2007, in From Stars to Galaxies: Building the Pieces to Build Up the Universe, Astronomical Society of the Pacific Conference Series, vol. 374, eds. A. Vallenari, R. Tantalo, L. Portinari, & A. Moretti, 409
Ivezić, Ž., Sesar, B., Jurić, M., et al. 2008, ApJ, 684, 287
Jofré, P., Panter, B., Hansen, C. J., & Weiss, A. 2010, A&A, 517, A57
Jofre, P., & Weiss, A. 2011, arXiv: 1105.2022
Jurić, M., Ivezić, Ž., Brooks, A., et al. 2008, ApJ, 673, 864
Katz, D., Soubiran, C., Cayrel, R., Adda, M., & Cautain, R. 1998, A&A, 338, 151
Koleva, M., Prugniel, P., Bouchard, A., & Wu, Y. 2009a, A&A, 501, 1269
Koleva, M., de Rijcke, S., Prugniel, P., Zeilinger, W. W., & Michielsen, D. 2009b, MNRAS, 396, 2133
Koleva, M., Prugniel, P., Ocvirk, P., et al. 2007, in IAU Symposium, vol. 241, eds. A. Vazdekis & R. F. Peletier, 183
Kurucz, R. L. 1993, SYNTHE spectrum synthesis programs and line data
Lastennet, E., Lejeune, T., Oblak, E., Westera, P., & Buser, R. 2002, Ap&SS, 280, 83
Le Borgne, D., Rocca-Volmerange, B., Prugniel, P., et al. 2004, A&A, 425, 881
Le Borgne, J.-F., Bruzual, G., Pelló, R., et al. 2003, A&A, 402, 433
Lee, Y. S., Beers, T. C., Sivarani, T., et al. 2008a, AJ, 136, 2022
Lee, Y. S., Beers, T. C., Sivarani, T., et al. 2008b, AJ, 136, 2050
Luo, A.-L., Wu, Y., Zhao, J., & Zhao, G. 2008, in Society of Photo-Optical Instrumentation Engineers (SPIE) Conference Series, vol. 7019
Luo, A.-L., Zhang, Y.-X., & Zhao, Y.-H. 2004, in Society of Photo-Optical Instrumentation Engineers (SPIE) Conference Series, vol. 5496, eds. H. Lewis & G. Raffi, 756
Makarova, L., Koleva, M., Makarov, D., & Prugniel, P. 2010, MNRAS, 406, 1152
Manteiga, M., Ordóñez, D., Dafonte, C., & Arcay, B. 2010, PASP, 122, 608
Martins, L. P., González Delgado, R. M., Leitherer, C., Cerviño, M., & Hauschildt, P. 2005, MNRAS, 358, 49
Michielsen, D., Koleva, M., Prugniel, P., et al. 2007, ApJ, 670, L101
Munari, U., Agnolin, P., & Tomasella, L. 2001, Baltic Astronomy, 10, 613
Munari, U., Sordo, R., Castelli, F., & Zwitter, T. 2005, A&A, 442, 1127
Murphy, T., & Meiksin, A. 2004, MNRAS, 351, 1430
Noguchi, K., Aoki, W., Kawanomoto, S., et al. 2002, PASJ, 54, 855
Percival, S. M., & Salaris, M. 2009, ApJ, 703, 1123
Perryman, M. A. C., de Boer, K. S., Gilmore, G., et al. 2001, A&A, 369, 339
Prugniel, P., Koleva, M., Ocvirk, P., Le Borgne, D., & Soubiran, C. 2007a, in IAU Symposium, vol. 241, eds. A. Vazdekis & R. F. Peletier, 68
Prugniel, P., & Soubiran, C. 2001, A&A, 369, 1048
Prugniel, P., & Soubiran, C. 2004, arXiv: astro-ph/0409214
Prugniel, P., Soubiran, C., Koleva, M., & Le Borgne, D. 2007b, arXiv: astro-ph/0703658
Prugniel, P., Vauglin, I., & Koleva, M. 2011a, A&A, 531, 165
Prugniel, P., et al. 2011b, in preparation
Ramsey, L. W., Adams, M. T., Barnes, T. G., et al. 1998, in Society of Photo-Optical Instrumentation Engineers (SPIE) Conference Series, vol. 3352, ed. L. M. Stepp, 34
Re Fiorentin, P., Bailer-Jones, C. A. L., Lee, Y. S., et al. 2007, A&A, 467, 1373
Recio-Blanco, A., Bijaoui, A., & de Laverny, P. 2006, MNRAS, 370, 141
Rockosi, C., Beers, T. C., Majewski, S., Schiavon, R., & Eisenstein, D. 2009, in astro2010: The Astronomy and Astrophysics Decadal Survey, Science White Papers, vol. 2010, 14

Rodríguez-Merino, L. H., Chavez, M., Bertone, E., & Buzzoni, A. 2005, ApJ, 626, 411
Sánchez-Blázquez, P., Peletier, R. F., Jiménez-Vicente, J., et al. 2006, MNRAS, 371, 703
Schiavon, R. P., & Majewski, S. R. 2010, in IAU Symposium, 262, eds. G. Bruzual & S. Charlot, 428
Sharina, M. E., Chandar, R., Puzia, T. H., Goudfrooij, P., & Davoust, E. 2010, MNRAS, 405, 839
Sheinis, A. I., Bolte, M., Epps, H. W., et al. 2002, PASP, 114, 851
Shkedy, Z., Decin, L., Molenberghs, G., & Aerts, C. 2007, MNRAS, 377, 120
Short, C. I., & Hauschildt, P. H. 2010, ApJ, 718, 1416
Siebert, A., Williams, M. E. K., Siviero, A., et al. 2011, AJ, 141, 187
Singh, H. P., Gulati, R. K., & Gupta, R. 1998, MNRAS, 295, 312
Smirnova, A., & Moiseev, A. 2010, MNRAS, 401, 307
Smolinski, J. P., Lee, Y. S., Beers, T. C., et al. 2011, AJ, 141, 89
Sordo, R., Vallenari, A., Tantalo, R., et al. 2010, Ap&SS, 328, 331
Soubiran, C., Bienaymé, O., & Siebert, A. 2003, A&A, 398, 141
Soubiran, C., Odenkirchen, M., & Le Campion, J.-F. 2000, A&A, 357, 484
Steinmetz, M., Zwitter, T., Siebert, A., et al. 2006, AJ, 132, 1645
Su, D. Q., Cui, X., Wang, Y., & Yao, Z. 1998, in Society of Photo-Optical Instrumentation Engineers (SPIE) Conference Series, vol. 3352, ed. L. M. Stepp, 76
Tonry, J., & Davis, M. 1979, AJ, 84, 1511
Tull, R. G. 1998, in Society of Photo-Optical Instrumentation Engineers (SPIE) Conference Series, vol. 3355, ed. S. D'Odorico (Bellingham, WA: SPIE), 387
Valdes, F., Gupta, R., Rose, J. A., Singh, H. P., & Bell, D. J. 2004, ApJS, 152, 251
Valentini, M., & Munari, U. 2010, A&A, 522, A79
Vazdekis, A., Sánchez-Blázquez, P., Falcón-Barroso, J., et al. 2010, MNRAS, 404, 1639
Vogt, S. S., Allen, S. L., Bigelow, B. C., et al. 1994, in Society of Photo-Optical Instrumentation Engineers (SPIE) Conference Series, vol. 2198, Instrumentation in Astronomy VIII, eds. D. L. Crawford & E. R. Craine (Bellingham, WA: SPIE), 362
Wilhelm, R., Beers, T. C., & Gray, R. O. 1999, AJ, 117, 2308
Willemsen, P. G., Hilker, M., Kayser, A., & Bailer-Jones, C. A. L. 2005, A&A, 436, 379
Wu, Y., Singh, H. P., Prugniel, P., Gupta, R., & Koleva, M. 2011, A&A, 525, A71
Wylie-de Boer, E., & Freeman, K. 2010, in IAU Symposium, vol. 262, eds. G. Bruzual & S. Charlot, 448
Wyse, R. F. G. 2006, Mem. Soc. Astron. Italiana, 77, 1036
Xing, X., Zhai, C., Du, H., et al. 1998, in Society of Photo-Optical Instrumentation Engineers (SPIE) Conference Series, vol. 3352, ed. L. M. Stepp, 839
Yanny, B., Rockosi, C., Newberg, H. J., et al. 2009, AJ, 137, 4377
York, D. G., Adelman, J., Anderson, J. E., Jr., et al. 2000, AJ, 120, 1579
Zacharias, N., Finch, C., Girard, T., et al. 2010, AJ, 139, 2184
Zhao, M. F., Yang, J. F., Wu, Y., & et al. 2006, Third International Symposium on Neural Networks, Chengdu, China, proceedings 361-368 *Link: http://www.springerlink.com/content/y3up573088731544/*
Zhao, Y. 2000, in Society of Photo-Optical Instrumentation Engineers (SPIE) Conference Series, vol. 4010, ed. P. J. Quinn, 290
Zhu, Y., Hu, Z., Zhang, Q., Wang, L., & Wang, J. 2006, in Society of Photo-Optical Instrumentation Engineers (SPIE) Conference Series, vol. 6269, 20
Zwitter, T., Munari, U., & Siebert, A. 2005, in The Three-Dimensional Universe with Gaia, ESA Special Publication, vol. 576, eds. C. Turon, K. S. O'Flaherty, & M. A. C. Perryman, 623
Zwitter, T., Siebert, A., Munari, U., et al. 2008, AJ, 136, 421